A constitutive law for low-temperature creep of water-saturated sandstones

JOURNAL OF GEOPHYSICAL RESEARCH, VOL. 106, NO. B10, PAGES 21,811–21,826, OCTOBER 10, 2001

A constitutive law for low-temperature creep of water-saturated sandstones

Bryne T. Ngwenya, Ian G. Main, and Stephen C. Elphick
Department of Geology and Geophysics, University of Edinburgh, Edinburgh, Scotland, UK

Brian R. Crawford
ExxonMobil Upstream Research Company, Houston, Texas, USA

Brian G. D. Smart
Department of Petroleum Engineering, Heriot-Watt University, Edinburgh, Scotland, UK

Abstract. An accurate predictive model for the long-term strength of the continental lithosphere is important in a range of geophysical and geodynamic problems. While laboratory experiments are consistent with Mohr-Coulomb brittle faulting in the cold, upper continental crust, there is increasing evidence that time-dependent processes may also be important in these rocks, even at low temperature. However, there is some ambiguity as to the exact form of the constitutive law for describing time-dependent behavior of upper crustal rocks. Here we present results of room temperature creep experiments on a suite of water-saturated sandstones spanning a range of petrophysical and rheological properties and underlying deformation mechanisms. On physical and microstructural grounds our analysis suggests that a modified power law creep, of the form $\dot{\varepsilon} = A'(\sigma_d - \sigma_f)^{\eta'}$, where σ_d is the differential stress and σ_f is the long-term failure (fundamental) strength, provides a more complete description of the experimental data. In particular, the parameters can be used to differentiate between sandstone types, with A', σ_f, and η' varying systematically with cementation state, rock rheology, and confining pressure. The fundamental strength (σ_f) for time-dependent deformation varies much more than the other parameters of the distribution, making it a potentially sensitive indicator of underlying creep mechanisms. Further tests would be needed to prove the constitutive law on a wider range of rock types and to prove that the three-parameter model is statistically better in the general case.

1. Introduction

An accurate predictive model for the long-term strength of the continental lithosphere is important in a range of geophysical and geodynamic problems. Constitutive rules that are applied in such models are primarily based on laboratory experiments of rocks comprising the lithosphere. These experiments generally suggest Mohr-Coulomb brittle faulting in the cold, upper continental crust and plastic flow for the higher temperature, lower crust, and mantle lithosphere [e.g., *Sibson*, 1977; *Goetze and Evans*, 1979; *Brace and Kohlstedt*, 1980; *Kirby and Kronenberg*, 1987; *Kohlstedt et al.*, 1995]. However, laboratory experiments also show that time-dependent deformation is important in rocks even at low temperature. For example, the presence of chemically active pore fluids such as water produces time-dependent failure at stresses much lower than those obtained from standard dry strength tests [e.g., *Griggs*, 1940; *Scholz*, 1968; *Kranz*, 1980; *Costin*, 1987; *Lockner and Byerlee*, 1980; *Lockner*, 1993, 1998]. This time-dependent deformation in the brittle field is important for understanding the long-term behavior of the Earth's lithosphere. In particular, seismogenic faulting does not always match the observed geological strain, implying a finite contribution from time-dependent creep mechanisms in microscopically brittle rocks. Thus time-dependent deformation plays an important role in the analysis of earthquake aftershocks and recurrence intervals [*Scholz*, 1968; *Main*, 2000]. In addition, the analyses of the stability of mine openings, boreholes, well casing, and hydrofractures in geothermal and hydrocarbon reservoirs are important engineering applications of creep rheology at higher strain rates [*Costin*, 1987].

Also solid-state creep is important in understanding compaction of sediments and sedimentary rocks following deposition and burial [*Dewers and Hajash*, 1995]. Previous studies have shown that under diagenetic conditions at low temperature but high pressures, granular aggregates such as sediments exhibit power law dependence between the strain rate and the applied differential stress, with a stress exponent of the order unity [*Rutter*, 1983; *Gratier and Guiget*, 1986; *Spiers et al.*, 1990; *Paterson*, 1995; *De Meer and Spiers*, 1995, 1997]. In these studies the aggregates deform predominantly by microscopically ductile processes [*Groshong*, 1988], including granular flow and diffusive mass transfer.

In contrast, low-temperature creep of crystalline rocks such as granites occurs by dilatant microcracking and is generally observed to follow an exponential dependence of strain rate on differential stress [*Scholz*, 1968; *Lockner*, 1993, 1998]. This difference suggests that the form of the macroscopic creep law

Paper number 2001JB000403.
0148-0227/01/2001JB000403$09.00

Table 1. Sample Properties[a]

Source	Mineralogy and Texture	Sample	Porosity, %	Cohesive Strength, MPa	Rheology
Gyda	generally dark and nodular (calcite and dolomite) and variably argillaceous (illite and muscovite); 69–75% quartz and 15–25% feldspar; grain size from 0.1 to 1.5 mm	GD-1	4.3	30	strongly cemented and brittle across whole range of confining pressures used (6.9–70 MPa)
		GD-2	20.0	22	
		GD-3[b]	15.0	29	
Magnus	medium- to coarse-grained sandstones (0.1–3 mm); consisting of quartz with subordinate orthoclase and albite; diagenetic minerals include kaolinite, dolomite, and pyrite	MG-1	26.9	15	brittle to ~48.2 MPa, followed by ductile behavior to 70 MPa confining pressure
		MG-2	26.1	11	
		MG-3[b]	25.5	16	
Gullfaks	fine-grained (0.05–0.3 mm), with detrital quartz, feldspar, and muscovite; cemented in up to 50% calcite	GF-1	20.9	15	ductile at all confining pressures above 6.9 MPa
		GF-2[b]	34.7	2.7	
		GF-3	27.3	4.8	
Scott	extremely coarse-grained (0.1–5 mm) quartzofeldspathic sandstones with extensive quartz overgrowth cements	SC-1	15.6	41	brittle across whole range of confining pressures
		SC-2[b]	11.1	45	

[a]Summary of rheological behavior of test samples and their mineralogical, petrophysical, and mechanical properties determined from short-term failure tests.

[b]Representative examples illustrating the derivation of constitutive equations throughout the paper. Data for other samples are available on request.

may be linked uniquely to the underlying microscopic deformation mechanism. However, *Lockner* [1993] showed that his creep data on Westerly granite could be described equally well by a power law relationship. Therefore, although the exact form of the constitutive law for low-temperature creep of such rocks is still debatable, the possibility that brittle rocks can also obey power law rheology suggests that the form of the law may not have any mechanistic significance. Rather, it may point to the existence of a universal constitutive equation for describing time-dependent behavior of upper crustal rocks. As shown by *Jin et al.* [1994] for olivine, the underlying micromechanical processes may be discerned from such an equation through differences in the magnitudes of the relevant material parameters, rather than the form of the constitutive parameters.

The objective of this communication is to report results from a suite of creep experiments designed to test this hypothesis for sandstones. Because of the natural variability in their mechanical properties, sandstones provide suitable material for investigating the existence of a universal constitutive law. As such, we set out to characterize the creep behavior of a suite of sandstones that are lithified to different degrees and hence display a variation in mechanical behavior ranging from brittle (well-cemented) to ductile (poorly cemented). Specific objectives of the study were (1) to develop an empirical law for creep of sandstones that can be applied to model their mechanical behavior; (2) to investigate the underlying micromechanical processes; and (3) to characterize the effects of environmental variables such as confining pressure and pore pressure.

We show that all sandstones examined in the present study can be described by the same macroscopic creep law, with underlying microscopic mechanisms that can be differentiated on the basis of the magnitude of a single material constant, the fundamental strength of the rock. Further work is required to demonstrate if the new law can provide a more general framework for the development of a rheological model for long-term behavior of crustal rocks.

2. Materials and Methods

2.1. Sources and Properties of Samples

Our experimental study was part of a wider investigation aimed at understanding the effects of stress on fluid flow in faulted reservoir sandstones. As a result, all our test samples were obtained from downhole core from four oil fields in the North Sea, namely, Gyda, Magnus, Scott, and Gullfaks oil fields. The mechanical behavior of sedimentary rocks is generally a function of porosity, mineralogical composition and/or degree of lithification/cementation. Our samples were therefore carefully selected to provide a broad range of mechanical and rheological properties. In general, high-porosity rocks deform by shear-enhanced compaction and granular flow at confining pressure above 100 MPa and hence display microscopically ductile behavior under such conditions [*Wong et al.*, 1997]. In addition, the presence of compliant minerals such as calcite and clays imparts a high degree of microscopic and macroscopic ductile behavior to sandstones [e.g., *Dunn et al.*, 1973]. Finally, samples that have undergone little lithification and/or cementation can also exhibit macroscopically ductile behavior, even at low confining pressures.

A summary of the important features of our test samples is given in Table 1. An important discriminator of the samples' mechanical behavior was their cohesive strength (defined as the intercept of a linear Mohr-Coulomb fracture strength envelope in normal stress versus shear stress space). As Table 1 shows, we found that a high cohesive strength was a good indicator of brittle behavior, while ductile samples were characterized by low cohesion and generally low degree of lithification. Samples showing some degree of ductile behavior at the low pressures investigated here ($P_c < 70$ MPa) also tended to have higher porosity and/or a higher percentage of compliant minerals (e.g., GF-2) than brittle ones. These mineralogical, mechanical, and/or rheological properties form the basis for our interpretation of the mechanical results and associated microstructural observations of the deformed samples.

2.2. Sample Preparation

All tests were carried out on cylindrical cores using a stiff testing flow rig in which confining pressure and axial load were varied independently using a high-pressure hand pump, with both pressures being kept constant by in-line bladder accumulators (Figure 1). The axial pressure is delivered by a 500-kN ram, while confining pressures up to 70 MPa can be applied to the cylindrical surface of core samples. Pore pressure is applied

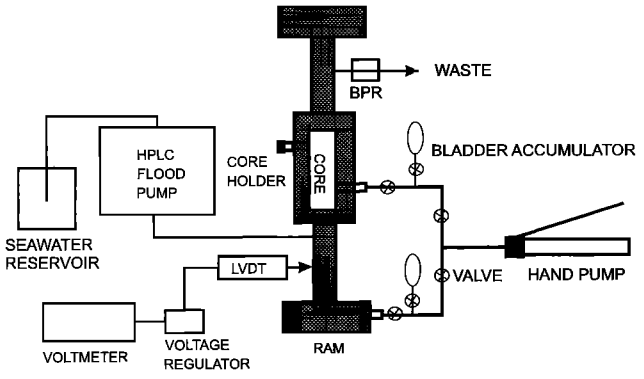

Figure 1. Schematic layout of the deformation rig, with manually operated pump for both confining pressure and axial pressure, both buffered with in-line bladder accumulators. The "waste" water downstream of the core passes through a backpressure regulator (BPR) that sets the pore pressure.

independently through a backpressure regulator at the down stream end of the core, with a maximum rating of 34.5 MPa.

Sample preparation consisted of coring right circular cylinders ranging in diameter from 0.033 to 0.038 m from reservoir whole core, followed by cleaning in acetone using the hot soxhlet method. This involves putting a core sample in a 41-mm-diameter Whatman Cellulose Extraction Thimble, which is then placed in a condenser connected to a flask containing acetone seating on a heating mantle. The boiling acetone condenses into and fills the thimble, eventually overflowing back into the flask and flushing the sample of oil in the process.

The sample diameter depended on the mechanical integrity of the whole core. For consolidated and mechanically strong sandstones, cores were made to 0.038-m-diameter, cut and faced off in a lathe and the end faces polished on 600 tungsten carbide grit. For loosely consolidated samples (Gullfaks only) the samples were cored to 0.033 m diameter, and after facing off on the lathe, they were capped in a wire mesh before soxhlet cleaning to prevent the cores from crumbling. After cleaning, these samples were wrapped in a soft heat-shrink plastic, bringing the circumference to the 0.038 m for the core holders that were used in the test program. These samples were not polished prior to loading in the core holder. Because all our samples were obtained from reservoir sandstones, the length to diameter ratio was fixed by the availability of downhole core to be in the range 2–2.5/1.

2.3. Experimental Procedure

Experiments were conducted using the so-called static fatigue method, where the rock sample is loaded to a constant stress that is lower than the short-term failure strength. In such an experiment the rock deforms according to a strain-time curve as shown schematically in Figure 2a. The initial loading of the sample produces an instantaneous elastic strain ε_0. Subsequently, the rock goes through a transient (primary) creep phase in which strain rate decreases with time. This is followed by a period of steady state or secondary creep where the strain rate is constant. Eventually, the rock goes into tertiary creep where strain rate increases nonlinearly with time until failure occurs at F.

We note in Figure 2b that depending on the stress magnitude, the rock is in steady state creep for much of the time that it takes for the sample to fail catastrophically. Because the strain rate is approximately constant during steady state creep, development of a constitutive relation between steady state creep rates and other variables is an important component in characterizing the full stress dependence of the creep cycle [*Lockner*, 1993]. Traditionally, this has been approached by conducting a series of creep tests where identical samples are subjected to systematic changes in external variables (Figure 2b) and the resulting steady state creep rate is measured [e.g., *Griggs*, 1940]. Because we used reservoir core, it was impractical for us to obtain sufficient identical samples for a complete experimental program. It is also debatable how "identical" such samples might be, given local variations in material and diagenetic properties. We thus adopted the "stress-stepping" method of *Lockner* [1993], where the same sample was subjected to step changes in differential stress and confining and pore pressures. This method has also been adopted recently by *Maranini and Brignoli* [1998] and shown to be reliable.

Clearly, the first step in such an experiment is to measure the rock's short-term failure strength in order to determine appro-

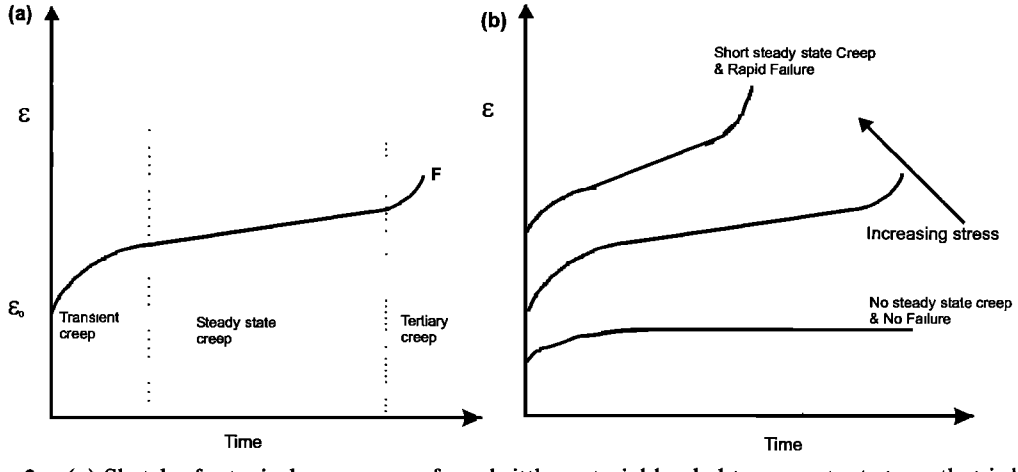

Figure 2. (a) Sketch of a typical creep curve for a brittle material loaded to a constant stress that is below short-term strength. The curve shows three different stages of deformation (labeled). Note that under these conditions, the rock spends most time in the steady state creep phase. (b) Illustration of typical creep curves for determining variation of steady state creep with differential stress. Note that below a certain stress, termed the fundamental strength, the rock does not attain steady state creep and will therefore never fail.

priate loading stresses for creep. These dynamic, short-term failure stresses were determined on a nominally dry sample cored from the same horizon as the creep test samples at different confining pressures using the multifailure state method. These dynamic results are not included in the line fits to the quasi-static creep test data described below because differences in the loading conditions produce different behavior [*Main*, 2000]. For the creep tests, each core sample was presaturated under vacuum in synthetic seawater [*Harrison et al.*, 1980] before being placed in the Hoek cell at a confining pressure of 13.8 MPa (2000 psi). The core was then loaded axially to 70% of its dry, short-term failure strength and left overnight to undergo primary creep at ambient pore pressure (0.1 MPa). This was necessary to ensure that all measured rates were in the steady state regime. During this conditioning phase (which lasted some 15 hours) and throughout the experiment, cores remained saturated by injecting synthetic seawater at a flow rate of 0.1 $cm^3\ min^{-1}$. Synthetic seawater was used instead of distilled water partly to prevent clay swelling but also to simulate deformation during seawater flooding, a common practice in late stage hydrocarbon recovery more generally.

The actual experiment consisted of varying the axial stress from 70 to 90% of the dry short-term failure strength while pore pressure and confining pressure were kept constant. Strain was measured at 1-min intervals using a linear voltage differential transducer (LVDT) mounted externally on the axial ram. After four to five axial stress changes, the confining pressure was increased in 6.9-MPa or 13.8-MPa intervals, and the measurements repeated until all the desired confining pressures were covered. The pore pressure was then increased and axial stress and confining pressure cycling repeated. Since the same sample was used to investigate the pore pressure dependence of creep, the differential stresses used at higher pore pressures were arbitrarily reduced to avoid the sample creeping to failure. Failure strengths are also a function of pore pressure, and since this dependence was not predetermined, the ratio of the differential stresses at higher pore pressures to the short-term strength could not be calculated accurately. For uniformity, therefore we have chosen not to normalize creep stresses to the dry short-term strength in our computations, as is often the case [e.g., *Kranz*, 1980]. In some cases, samples failed prematurely so that we could not collect the complete data at different confining and pore pressures. However, as will be shown in section 3.1, the general form of the constitutive law was found to be the same at all pressures investigated here.

Typical strain time data for an experiment at a single pore pressure but varying confining pressure are shown in Figure 3 for sample GD-3 (Gyda), where each strain step represents a step change in differential stress. These raw data were used to calculate steady state strain rates over the time interval for each axial stress. Invariably, a small component of transient creep was observed following each increase in stress, but a constant creep rate was eventually attained [*Lockner*, 1993]. In the derivation of strain rates we ignored the first few minutes during which transient creep was occurring. The resulting strain rates are subject to an estimated total error of about 3%.

Eventually, all our samples were allowed to creep to failure. Subsequently, the core was flushed with distilled de-ionized water, dried at 60°C for 1 week and then impregnated with epoxy resin while still encased in the rubber liner. After impregnation, whole thin sections were made perpendicular to the shear fractures, and the sections were used to study microstructural and fault gouge characteristics under polarized light microscopy.

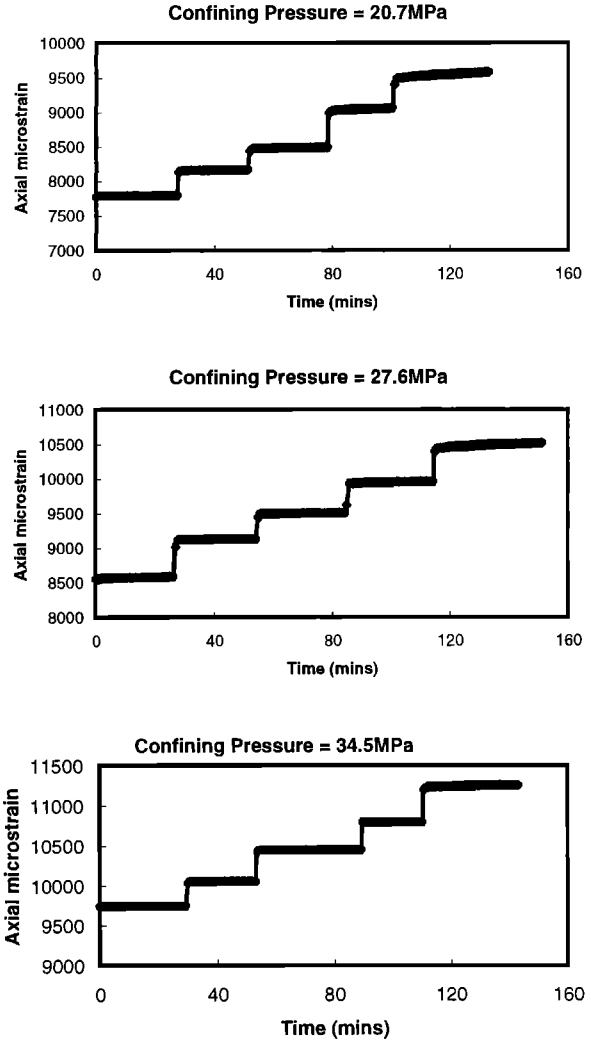

Figure 3. An example of the axial strain time raw data obtained during a "stress-stepping" experiment on a single core at different confining pressures and a constant pore pressure. The slope of each stress step provides a single strain rate data at each confining pressure.

3. Results

3.1. Mechanical Data

Strain rates calculated from the recorded strain time data are plotted against differential stress in Figure 4, where compressive stress is taken as positive. In general, we note that the data can be described by both a power law (Figure 4a)

$$\dot{\varepsilon} = A(\sigma_d)^{\eta} \tag{1}$$

and an exponential law (Figure 4b)

$$\dot{\varepsilon} = Ce^{\beta\sigma_d}, \tag{2}$$

where $\dot{\varepsilon}$ is the steady state strain rate, σ_d is the differential stress and A, C, β, and η are constants. Table 2 shows values of the constants A, C, η, and β obtained by curve-fitting (1) and (2) to the experimental data. The fitting was carried out using a nonlinear least squares routine based on the Marquardt-Levenberg algorithm [*Marquardt*, 1963]. The correlation coefficients, together with the residual sum of squares, were used to assess goodness of fit to the data. On the basis of

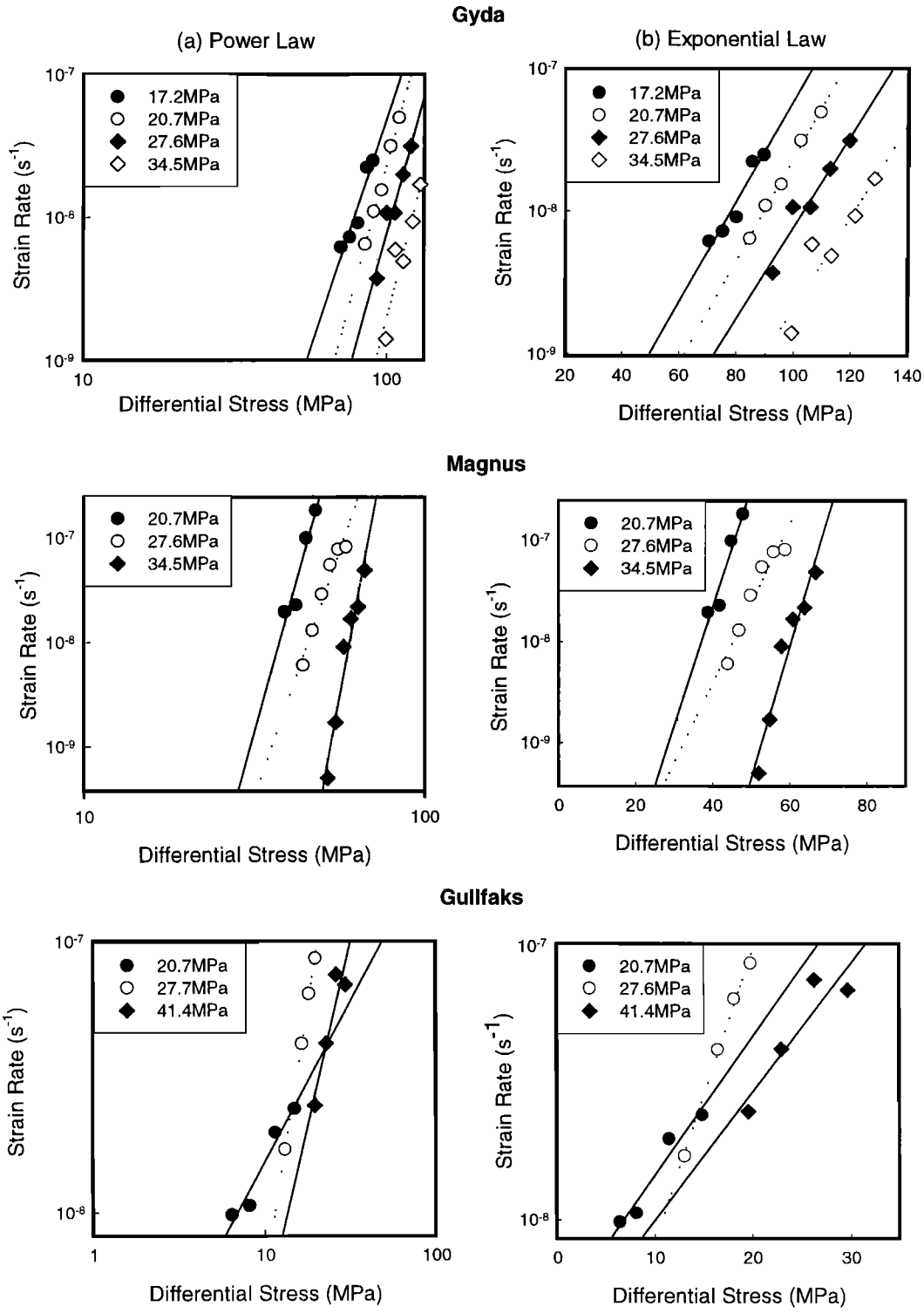

Figure 4. Representative graphs of strain rate plotted against differential stress for core samples from three sandstones (Gyda, Magnus, and Gullfaks) with contrasting mechanical properties and rheological behavior. For comparison, the data presented in each case are for a single pore pressure of 13.8 MPa, while the different symbols represent different confining pressures. Note that for each sample, both (a) power and (b) exponential laws adequately fit the data. In all cases, there is a tendency for the curves to shift to the right (lower strain rate) with increasing confining pressure, although this shift is not robust for the ductile Gullfaks sandstones.

these criteria, we found that 92% (11/12) of Gyda, 64% (7/11) of Magnus, and 38% (3/8) of Gullfaks data are better fit with the exponential equation. Thus, while both constitutive laws fit the data for all three reservoir rocks, the exponential form provides a better mathematical description for more brittle (Gyda and Magnus) samples, while the power law form is more suitable for ductile samples.

Because of the large volume of data we have chosen a single

Table 2. Regression Constants for Power (Equation (1)) and Exponential (Equation (2)) Fits to the Experimental Data for Gyda, Magnus, and Gullfaks Samples Shown in Figure 4[a]

Pore Pressure, MPa	Confining Pressure, MPa	Power Law (Equation (1))			Exponential Law (Equation (2))		
		A, $MPa^{-\eta}\ s^{-1}$	η	r^2	β, MPa^{-1}	C, s^{-1}	r^2
			Gyda Sample				
0.1	13.8	−18.7	5.72	0.990	0.06	−9.92	0.996
	20.7	−19.5	5.79	0.708	0.08	−11.7	0.810
	27.6	−20.2	5.99	0.912	0.06	−11.2	0.966
	34.5	−22.7	6.03	0.968	0.05	−10.7	0.967
6.9	13.8	−15.6	4.29	0.977	0.06	−9.67	0.973
	20.7	−19.9	60.7	1.000	0.07	−10.6	1.000
	27.6	−25.9	8.81	0.916	0.11	−13.3	0.983
	34.5	−28.1	9.72	0.852	0.12	−14.9	0.946
13.8	17.2	−23.9	9.56	0.975	0.16	−11.2	0.979
	20.7	−23.6	9.29	0.966	0.19	−12.2	0.985
	27.6	−24.9	9.61	0.969	0.19	−13.2	0.999
	34.5	−25.7	8.52	0.871	0.16	−13.8	0.999
			Magnus Sample				
0.1	13.8	−14.2	3.99	0.597	0.07	−8.94	0.594
	20.7	−19.3	6.60	0.870	0.11	−10.5	0.869
	27.6	−24.1	9.18	0.937	0.15	−11.5	0.949
	34.5	−23.7	8.90	0.938	0.15	−11.8	0.941
6.9	13.8	−20.0	7.54	0.984	0.23	−11.9	0.996
	20.7	−22.2	8.49	1.000	0.16	−11.3	1.000
	27.6	−21.0	7.59	0.947	0.18	−12.0	0.958
	34.5	−13.8	3.56	0.922	0.06	−9.02	0.932
13.8	20.7	−26.2	11.6	0.976	0.26	−12.1	0.973
	27.6	−25.3	10.4	0.964	0.18	−11.4	0.963
	34.5	−32.8	14.0	0.951	0.20	−13.2	0.958
			Gullfaks Sample				
0.1	13.8	−9.02	1.89	0.913	0.14	−7.70	0.874
	27.6	−7.60	0.60	0.837	0.04	−7.13	0.876
	41.4	−8.35	1.19	0.968	0.06	−7.34	0.981
6.9	13.8	−9.67	2.14	0.904	0.16	−8.25	0.861
	27.6	−8.51	1.07	0.667	0.22	−8.27	0.746
	41.4	NC	NC	NC	NC	NC	NC
13.8	20.7	−9.10	1.27	0.966	0.12	−8.40	0.920
	27.6	−12.7	4.37	0.997	0.26	−9.26	0.992
	41.4	−10.0	1.99	0.828	0.08	−8.17	0.806

[a]The data are for a single sample tested at different pore pressures and are representative of all our samples. On the basis of correlation coefficients, the exponential law provides a better mathematical description of the data for the brittle samples, while the power law is more suited to ductile samples. NC stands for no correlation.

sample from each reservoir to illustrate the general behavior (see Table 1). Table 2 shows values for the different constants and the associated regression coefficients in (1) and (2) for these representative samples. These values, differentiated according to the imposed pore pressure, have been plotted against confining pressure in Figures 5a–5c. The errors associated with these parameters during the fitting procedure were <10% for A and C and <5% for η and β. There are no values for Scott samples because no significant creep deformation was detected in the two samples that were tested (see later). From Figure 5 we note that there is a small confining pressure dependence to the constants A and C. Constant A (equation (1)) generally decreases with increasing confining pressure for the brittle sandstones, but is practically constant for ductile samples (Figure 5a). The decrease with confining pressure is particularly strong for the more brittle samples from Gyda, where this trend holds at all pore pressures used. A similar trend is observed for the dependence of C (equation (2)) on confining pressure, where the correlation is stronger for the more brittle samples (Figure 5b). In contrast, the stress exponent η (equation (1)) shows a slight increase for brittle samples and decreases slightly for ductile samples as the confining pressure increases (Figure 5c). In the case of A and C the highest values recorded are for the ductile samples, while these rocks give the lowest values for the stress exponent. In general, we find that $3 < \eta < 15$ for brittle and intermediate samples and $1 < \eta < 6$ for ductile sandstones. For the exponential law, β is mostly independent of both confining pressure and pore pressure (although a decrease with confining pressure is evident in the ductile Gullfaks sample). It varies from 0.04 to 0.26 MPa^{-1}, with an average of 0.13 ± 0.06 (Figure 5d), where the error is 1 standard deviation. There is no significant difference in β between the brittle and ductile sandstones. The observed variations in the confining pressure dependence of the material constants implies that the power law form may be more sensitive to differences in rheological attributes of the sandstones, while the exponential form provides a better statistical model for the data presented here.

The effect of confining pressure is to shift the individual curves of strain rate systematically toward higher differential stresses (Figure 4), implying a reduction in strain rate with confining pressure at a given differential stress [*Griggs*, 1940; *Robertson*, 1960; *Kranz*, 1980]. However, the exact form of the dependence of creep on confining pressure cannot be estab-

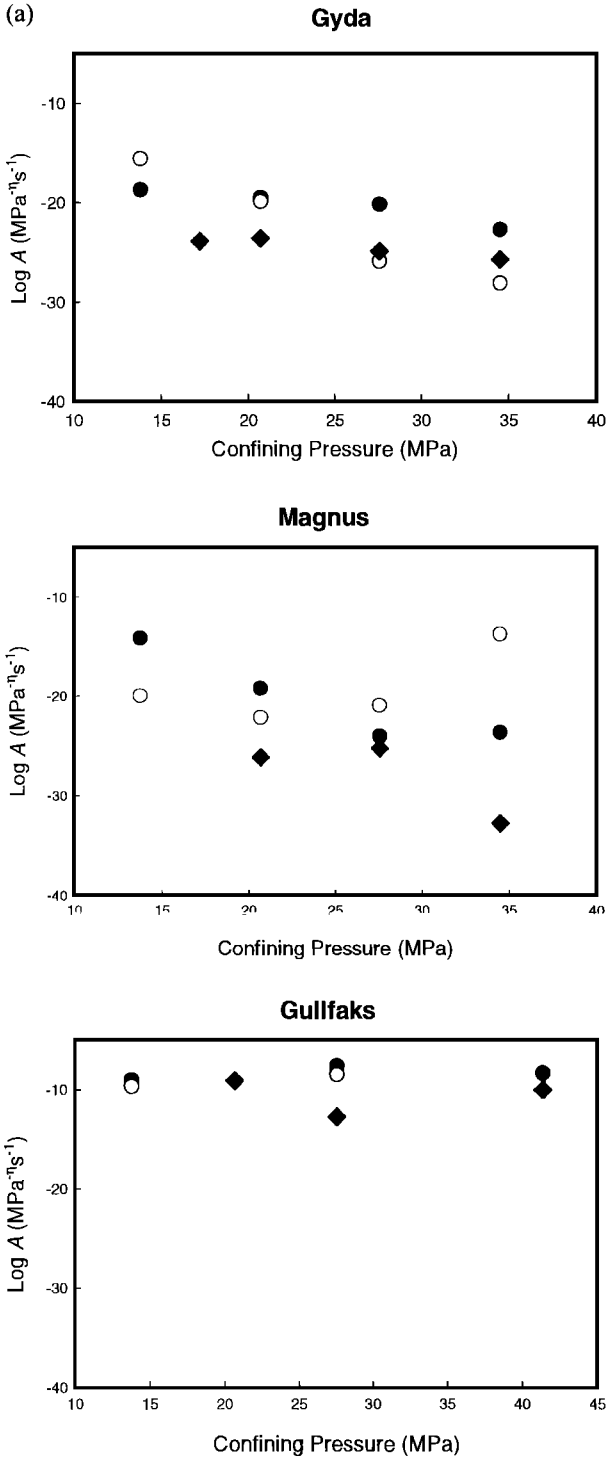

Figure 5a. Confining pressure dependence of the material constants in the power law (equation (1)) and exponential law (equation (2)). The more brittle Gyda samples often show a strong confining pressure dependence to the constant A. Solid circles, 0.1 MPa; open circles, 6.9 MPa; solid diamonds, 13.8 MPa. Other samples also show small confining pressure sensitivity to A, η (Figure 5c), and C (Figure 5b) (see text for details), while β (Figure 5d) does not depend on confining pressure.

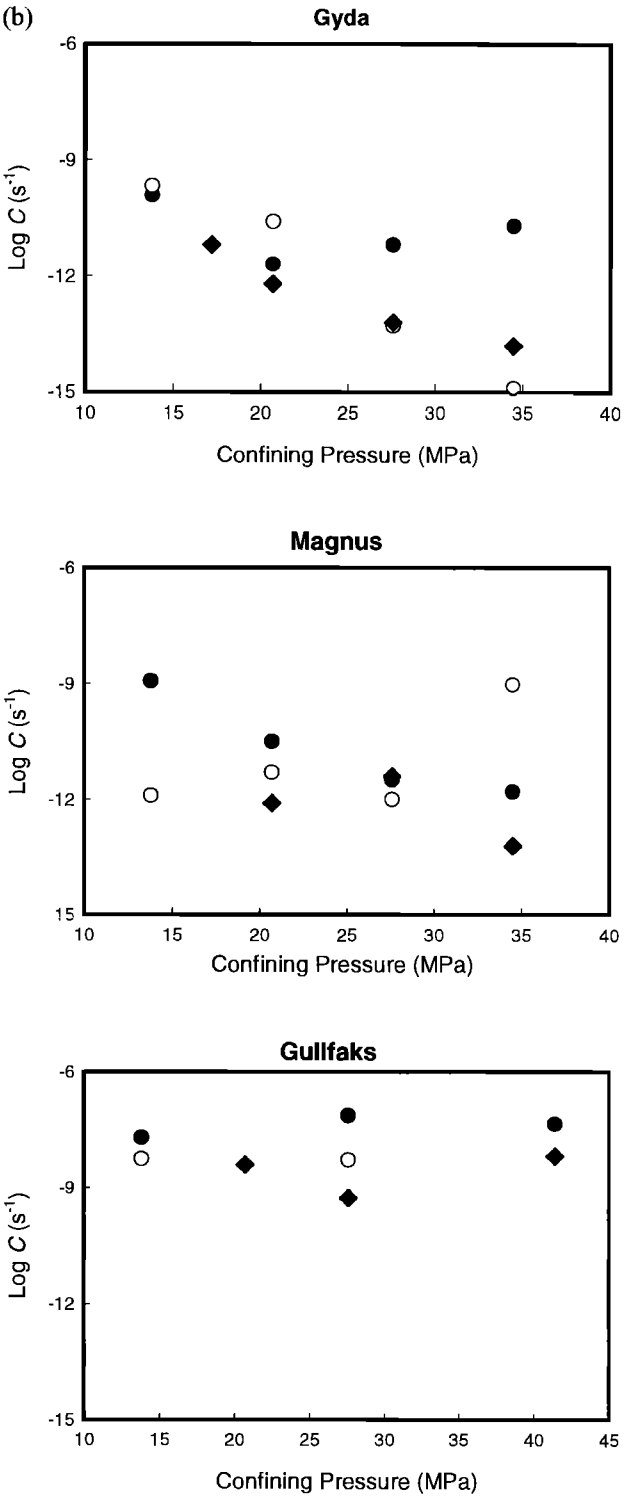

Figure 5b. Same as Figure 5a except for C.

lished from the few data presented here. This warrants further investigation, particularly as it is likely to change the mechanism of creep from microcracking to pressure solution [*Rutter and Mainprice*, 1978; *Kranz*, 1980].

An increase in pore pressure is expected to accelerate stress corrosion and hence creep rates for brittle samples, which may manifest in the form of a higher stress exponent (η) [*Atkinson and Meredith*, 1987]. This behavior is qualitatively demonstrated in Tables 2a and 2b, where the values of η are higher for the 13.8 MPa pore pressure than those for both 0.1 MPa and 6.9 MPa pore pressures at a given confining pressure. In contrast, pressure solution creep increases with increasing effective stress [*Dewers*

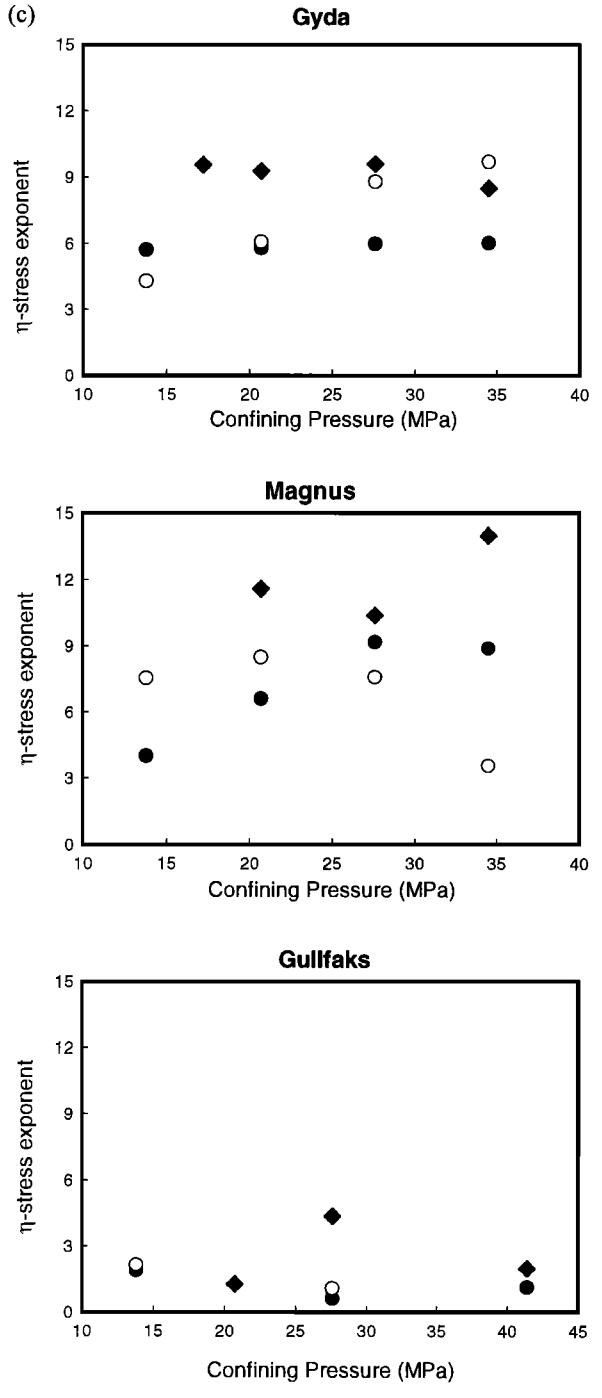

Figure 5c. Same as Figure 5a except for η.

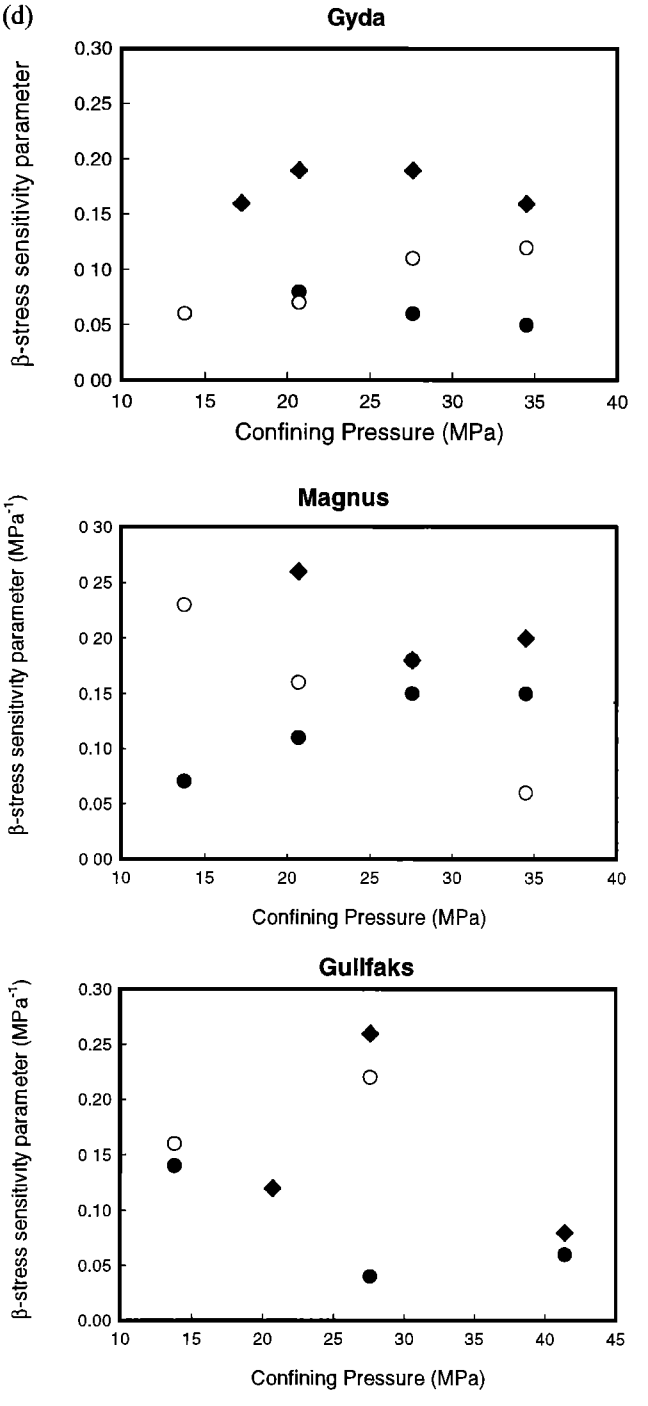

Figure 5d. Same as Figure 5a except for β, which is independent of confining pressure.

and Hajash, 1995], so the effect of increased pore pressure may well be to reduce compaction creep under higher effective pressures than considered here. Under these high pressures, power law creep is also observed, with a stress exponent of about unity [e.g., *Rutter*, 1983]. In general, however, the range of pore pressures used is too limited, so that we are not able to draw meaningful conclusions about the effect of pore pressure.

In summary, analysis of the mechanical data reveals that on statistical grounds the exponential law fits the creep data better for brittle samples, while the power law form is better for ductile samples. However, the material constants for the power law form show a stronger dependence on sample rheology and are more sensitive to external variables.

3.2. Posttest Microstructural Observations

In all cases, our samples were eventually allowed to creep to failure. Thin sections made from epoxy-impregnated, fractured samples were examined for microstructural characteristics using polarized light microscopy. The main objective was to provide a qualitative description of the nature of the shear fractures developed in terms of their width, grain characteristics,

and associated microfractures in order to characterize microscopic deformation mechanisms, albeit for a snapshot at the end of the such tests. In our previous studies we have found that scanning electron microscopy, particularly in backscattered mode is required to quantify microfractures in deformed samples [*Ngwenya et al.*, 2000]. However, polarized light microscopy provided sufficient resolution for identifying microfractures, and other studies have also shown that microfractures of ~3 μm long can be resolved by this technique [e.g., *Moore and Lockner*, 1995].

Figure 6 shows thin sections of four of the samples, each representing one of the sandstones tested for this study; all taken at the same magnification (X10) to facilitate comparison. The photomicrographs used have deliberately been chosen to emphasize the nature and type of microcracks associated with the macroscopic fractures. In all cases, the σ_1 direction is vertical. Figure 6a is a thin section for a sample from the Gyda sandstone, which failed by formation of a single shear fracture, oriented ~37° from the principal stress direction (σ_1). However, there was also a small dilatational fracture that was almost parallel to σ_1. The main shear zone averages 0.5 mm thick but occasionally reaches 1 mm in places. Within the shear zone itself, intense cataclasis has resulted in reduced grain size (grain size of ~1 μm), but large grains are also present, although these appear fractured. As evident from Figure 6a, there is a fringe of microcracks adjacent to the main shear zone. The population of microcracks comprises a mixture of grain boundary and extensional microcracks, the latter being either intragranular or transgranular. The microcrack fringe can be as wide as 2 mm in place, equivalent to about five grain diameters. Examination of the thin section away from the shear fracture shows reduced microcracks, which are randomly oriented and bear no relation to the direction of the principal stress axis.

Figure 6b shows a thin section for a sample of the Magnus sandstone. As with the Gyda sandstone, this sample failed predominantly by the formation of a single, throughgoing shear fracture oriented at 30° to the principal stress direction. A second fracture, also inclined 30° to σ_1, was conjugate to the throughgoing fracture but terminated against the main fracture. The photomicrograph only shows a part of one of the shear fractures (northeast corner), which can be seen to carry what appears to be a whole grain. Both fractures are slightly thicker than those in Gyda sandstone cores, averaging 1.5 mm in thickness. As shown in Figure 6b, the shear fracture is associated with a fringe of axial microcracks, which are ubiquitous up to 1 mm away from the shear faults. Once again, a mixture of transgranular and intragranular cracks is present, with some of the latter initiating at pores.

In complete contrast to the Gyda and Magnus sandstones, thin sections for Gullfaks sandstone cores (Figure 6c) are characterized by a much wider, but diffuse shear zone inclined at ~40° to σ_1. Because of the abundant calcite cement in this rock, the shear zone appears almost opaque in the photomicrograph [see also *Dunn et al.*, 1973], but note that the center of the zone itself has been stripped of all loose fragments during the resin impregnation process, and is now filled with epoxy. This shear zone terminated within the sample and occasionally displayed some branching, but the most significant difference with the other samples is the complete lack of a microcrack fringe.

Finally, Figure 6d shows a thin section of the Scott sandstone, with the shear fracture showing only near the northeast corner of the photomicrograph. The shear fracture was generally narrower than those observed in the Gyda and Magnus cores and showed a zigzag pattern typical of fractures in low porosity crystalline rocks [e.g., *Moore and Lockner*, 1995]. As can be seen in the photomicrograph, there are abundant transgranular and intergranular microcracks, the former being parallel to the principal compressive stress. These microcracks are evident up to 3 mm away from the main shear fracture and in places up to 1.5 cm away.

In general, these studies point to subtle differences in the nature and spatial distribution of microcracks associated with macroscopic shear fractures. Notably, three of the four sandstones tested showed significant development of microcracks around shear fractures. We discuss these observations and intersandstone differences below in order to identify subtle differences in microscopic processes responsible for macroscopic creep deformation.

4. Discussion

Our experiments covered a range of sandstones with different mechanical attributes. However, analysis of their time-dependent deformation has shown that all can be described by the same macroscopic laws, although distinction can be made on the basis of statistical parameters. It may be argued that this is a reflection of the narrow range of strain rates (2 orders of magnitude at the most) over the experimental range of stresses used. However, *Lockner* [1993] similarly could not resolve whether creep of Westerly granite followed power law or exponential creep despite his data covering a wider range of strain rates (4 orders of magnitude). *Lockner* [1993] chose exponential behavior, which he successfully used to model time-dependent failure of Westerly granite [see also *Lockner*, 1998]. An important conclusion of his work was the finding that the stress sensitivity parameter β was similar for rocks ranging from granites to sandstones, which he attributed to the same underlying creep mechanism, this being subcritical crack growth. Conversely, differences in material parameters will be a result of differing microscopic creep mechanisms. Before discussing our choice of the constitutive equation, we therefore need to establish what microscopic processes were responsible for creep in our samples. In the absence of syndeformation data on volumetric changes and microseismic activity, these processes will be inferred from microscopic observations reported above.

4.1. Micromechanics of Creep in Sandstones

There now exists a large body of evidence that the deformation of rocks at low temperatures and pressures occurs by two mechanisms broadly referred to as brittle faulting and ductile flow [*Scholz*, 1968; *Friedman and Logan*, 1970; *Dunn et al.*, 1973; *Engelder*, 1974; *Hirth and Tullis*, 1989; *Moore and Lockner*, 1995; *Rao and Kusunose*, 1995; *Menendez et al.*, 1996; *Wong et al.*, 1997]. The term ductile is often used in three different contexts [*Rutter*, 1986], including (1) the plastic deformation of single crystals, (2) homogeneous deformation or uniform flow, and (3) deformation over and above a specified amount of strain. Here we will use the term ductile in a macroscopic sense of homogeneous deformation where the underling microscopic processes include shear-enhanced compaction, granulation, and granular flow [see *Paterson*, 1995; *Hirth and Tullis*, 1989; *Menendez et al.*, 1996]. Macroscopically, these microscopic processes constitute cataclastic flow [*Engelder*, 1974]. Experimen-

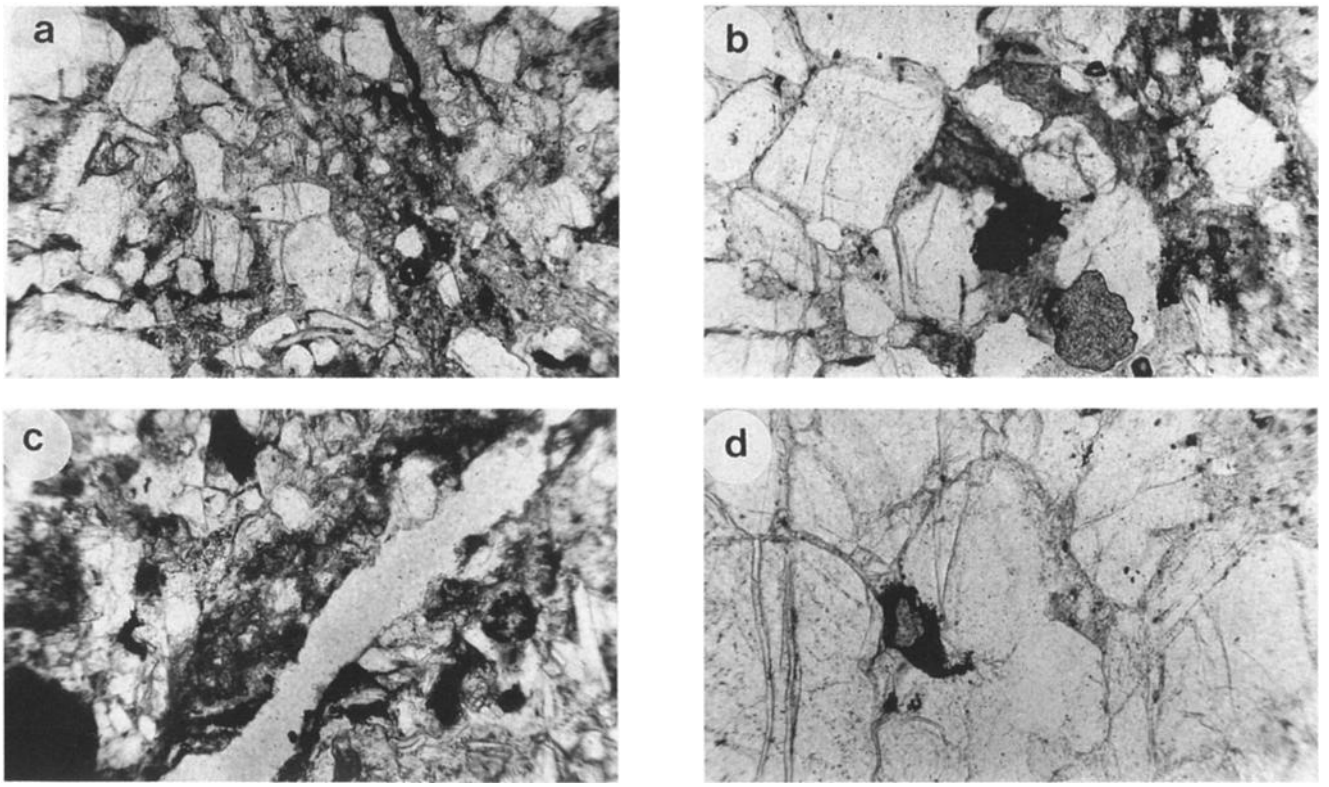

Figure 6. Photomicrographs of thin sections made perpendicular to fractures, showing microstructural characteristics associated with the fractures. (a) Gyda samples. Typically, these show relatively thin fractures fringed by grains that exhibit a mixture of grain boundary and extensional microcracks (intragranular and transgranular). (b) Magnus samples. The same textures are exhibited except that the shear zone here is slightly thicker than in the Gyda samples. (c) Gullfaks samples. These have a wider shear zone than both Gyda and Magnus samples, and the grains near the fracture exhibit no microcracking, consistent with ductile deformation. (d) Scott samples. In contrast, these are extremely brittle, have narrower fractures with typical zigzag patterns in places, and exhibit pervasive microcracking. All photos at X10 magnification.

tal evidence for cataclastic flow includes (1) the presence of a wide shear zone indicative of distributed damage and the presence of intact grains in gouge [*Dunn et al.*, 1973], (2) extensive pore collapse, often accompanied by intragranular microcracks that originate by "spalling" [*Hirth and Tullis*, 1989], and (3) local Hertzian fractures originating at grain-grain contacts [*Menendez et al.*, 1996].

In contrast to this distributed cataclastic flow, macroscopic brittle deformation at low effective pressures is characterized by dilatant microfracturing, which leads to shear localization along narrower fracture zones, often consisting of linked segments with a zigzag pattern [e.g., *Dunn et al.*, 1973; *Moore and Lockner*, 1995]. In thin sections, brittle fracture is evident from the presence of abundant microcracks in the vicinity of, and away from, the shear fracture [*Hirth and Tullis*, 1989; *Ngwenya et al.*, 2000]. Many of these microcracks are parallel to the principal compressive stress and may originate by axial splitting of intact grains [*Brace et al.*, 1966; *Scholz*, 1968; *Engelder*, 1974] or fracturing of grain boundaries [*Hirth and Tullis*, 1989; *Menendez et al.*, 1996].

From previous experimental studies, researchers are in agreement that for siliclastic sedimentary rocks, distributed cataclastic flow is the dominant failure mechanism in high porosity rocks, particularly at high mean effective stresses [e.g., *Hirth and Tullis*, 1989; *Menendez et al.*, 1996; *Wong et al.*, 1997]. Conversely, localized brittle fracture dominates in low porosity rocks, as well as in high-porosity rocks at low mean effective pressures. However, there has been a long-standing debate on the timing of the axial and grain boundary cracks relative to the macroscopic failure processes. *Friedman and Logan* [1970] noted the absence of microcracks around fractures along which there had been no shear displacement and argued that the microcracks formed after fracture. Similarly, *Engelder* [1974] interpreted the constant thickness of the damage zone (5–10 grain diameters) as indicating the progressive migration of the damage zone into the intact sample during shear. In contrast, microseismic measurements [e.g., *Lockner et al.*, 1992] and microscopic analysis of samples deformed to stresses just under the failure strength [e.g., *Hirth and Tullis*, 1989; *Menendez et al.*, 1996] suggest that significant microcracking occurs prior to failure. In particular, acoustic emission monitoring has revealed the progressive development of microcracking from a pervasive to a localized process as samples approach failure in both constant strain rate and/or creep experiments [*Lockner et al.*, 1992; *Glover et al.*, 1996]. *Menendez et al.* [1996] have attempted to reconcile these differences by suggesting that prefailure microcracks in low-porosity sandstones and crystalline rocks originate from loss of grain boundary cohesion.

From section 3.2 we noted that the samples of Gyda and Magnus sandstones failed by throughgoing shear fractures, which were associated with abundant microcracks. These microcracks were concentrated in the vicinity of the shear zone. Such distribution is well known and quantitative analysis has also shown that the number of microcracks per unit area de-

Table 3. Rheological Constants for Equation (3) for Gyda, Magnus, and Gullfaks Samples[a]

Pore Pressure, MPa	Confining Pressure, MPa	σ_f, MPa	Log A', MPa$^{-\eta'}$ s^{-1}	η'	r^2	AIC_2	AIC_3
			Gyda Sample				
0.1	13.8	33.2	−14.5	3.98	0.991	−97	−98.1
	20.7	52.3	−16.5	4.94	0.770	−90.3	−91.9
	27.6	60	−15	4.04	0.941	−94.5	−96.5
	34.5	80	−12.9	2.98	0.965	−97.9	−98.8
6.9	13.8	39.5	−10.4	1.84	0.979	−101	−102
	20.7	50	−12.8	2.99	1.000	−100	−101
	27.6	70.1	−17.9	6.00	0.971	−91.6	−95.2
	34.5	95.2	−17.4	6.02	0.930	−87.8	−90.7
13.8	17.2	35.3	−12.4	3.98	0.968	−88.1	−88.5
	20.7	31.3	−14.5	5.07	0.976	−74.9	−76.6
	27.6	51	−12.5	4.04	0.998	−71.5	−78.5
	34.5	56.1	1.14×10^{-16}	4.39	1.000		
			Magnus Sample				
0.1	13.8	22.0	−10.3	1.97	0.624	−90.9	−92.1
	20.7	25.2	−13.3	3.72	0.868	−112	−113
	27.6	27.9	−15.7	5.24	0.925	−113	−114
	34.5	32.0	−14.9	4.85	0.943	−112	−113
6.9	13.8	21.0	−13.1	4.04	0.991	−122	−125
	20.7	27.8	−11.2	2.44	1.000	−119	−120
	27.6	33.3	−12.1	3.22	0.969	−137	−140
	34.5	38.0	−9.24	1.30	0.904	−97.5	−97.9
13.8	20.7	32.6	−10.6	3.23	0.980	−72.8	−74.2
	27.6	38.4	−10.0	2.36	0.991	−93.4	−97.9
	34.5	43.4	−12.5	3.79	0.949	−113	−114
			Gullfaks Sample				
0.1	13.8	9.18	−7.17	0.53	0.971	−88.4	−78.0
	27.6	0	−7.68	0.65	0.841	−93.3	−94.3
	41.4	0	−11.8	2.96	0.975	−94.6	−96.3
6.9	13.8	7.91	−7.69	0.63	0.986	−91.2	−97.0
	27.6	0	−8.49	1.04	0.667	−94.1	−95.1
	41.4	NC	NC	NC	NC	NC	NC
13.8	20.7	1.86	−8.74	1.02	0.974	−100	−102
	27.6	7.30	−9.76	2.48	0.996	−98.8	−98.8
	41.4	8.09	−8.85	1.32	0.832	−90.7	−91.8

[a]These constants were obtained by fitting the data to equation (3) using a nonlinear least squares routine [*Marquardt*, 1963]. AIC stands for Akaike information criterion, which attempts to penalize mathematical models for the number of adjustable parameters, based on the residual sum of squares. NC stands for no correlation.

creases exponentially with increasing distance away from the fracture trace [e.g., *Moore and Lockner*, 1995; *Ngwenya et al.*, 2000]. Many of these microcracks were either transgranular or intergranular and were mostly parallel to the principal compressive stress. Some intact grains were present in the shear zone, and a few of the microcracks were intragranular and consistent with origin as local Hertzian fractures.

Microstructural studies of the samples of the Scott sandstone were consistent with pervasive microcracking. However, the shear zone was found to be narrower than those found in Gyda and Magnus sandstones and had zigzag patterns typical of low porosity crystalline rocks [*Moore and Lockner*, 1995]. The localized faulting, coupled with pervasive distribution of microcracks, suggests that the axial microcracks away from the fracture trace may not be directly related to the formation of the fracture but may have formed earlier during creep. In contrast, samples from Gyda and Magnus sandstones showed local Hertzian fractures and spalling, and there were few microcracks away from the fracture, suggesting that the microcracks near the fracture formed during localization of the fracture, while creep was compaction dominated. Samples from these three sandstones thus appear to define progressive increase in the degree of microscopic brittleness from Magnus to Gyda to Scott, consistent with the increases in η from the rheological results. Furthermore, the presence of microcracks, which are remote from the shear fractures in the Scott samples suggests that their formation was not necessarily linked to the formation of the macroscopic fracture during tertiary creep. As such, our data are consistent with some of the microcracks preceding dilatant shear localization (steady state creep), while microcracks adjacent to the shear fracture may form during tertiary creep or postshear. *Mair et al.* [2000] reached similar conclusions from their study of microcrack distributions associated with the formation of multiple deformation bands in high-porosity sandstones.

In contrast to the three sandstones discussed above, Gullfaks sandstone cores failed by a diffuse shear zone that terminated within the sample and was characteristically lacking in microcracks. This characteristic ductile behavior may be due to the high porosity, combined with the presence of calcite cement, which makes up ~40–50% of the rock. Calcite is a compliant phase and is well known for imparting ductile behavior to siliclastic rocks [*Dunn et al.*, 1973; *Menendez et al.*, 1996].

The important conclusion from these results is that in brittle samples, a significant fraction of microcracks can form prior to shear localization and are therefore believed to be the under-

lying mechanism of creep [see also *Scholz*, 1968]. In contrast, the microcracks in less brittle samples may have formed as a result of shear localization during tertiary creep, suggesting that prior to fracture compactive processes dominated creep. Thus our sample suite includes a range of sandstones, which have been shown to creep by different microscopic processes. The latter can be attributed to differences in petrophysical properties of the rocks, as well as material properties of the minerals and cements in the rock. Despite these large differences, all our samples exhibited the same constitutive behavior. From these findings, we suggest that the form of the macroscopic constitutive equation is not necessarily indicative of the underlying macroscopic creep mechanism. It follows that the similarity in the value of the stress sensitivity parameter (β) observed here and by *Lockner* [1993] is not necessarily indicative of the same microscopic creep mechanism. This is important since *Lockner* [1993] calculated similar β values for data from *Rutter and Mainprice* [1978] for which pressure solution rather than localized microcracking was known to be the dominant creep mechanism. In contrast, we have found that the range of A and η for power law creep differ significantly between brittle and ductile samples, suggesting that they may reflect different underlying creep mechanisms. However, because we did not measure volumetric strain, it is not possible to confirm whether deformation was predominantly dilatant for brittle samples and compactant for ductile ones. We will address this important question in our future experiments.

4.2. A Modified Power Law Constitutive Equation

In this section, we attempt to develop a constitutive law for reservoir rocks based on mechanical data and a recent theoretical study by *Main* [2000]. Our primary motivation is to find a single law that satisfies several criteria. These include (1) providing an adequate statistical description of the experimental data, (2) having a physical basis, and (3) being able to discriminate between sandstones of different mechanical attributes and their response under different environmental conditions (confining pressure, pore pressure, and fluid chemistry). In our studies, confining pressure and pore pressure were varied while fluid chemistry was fixed by continuously flowing the same solution through the cores during the experiment.

In the case of the first requirement, we have shown that both exponential and power laws provide adequate mathematical descriptions of the experimental data. Further, we have shown that the exponential law is a better model for brittle materials at low confining pressures, while the power law is better for ductile materials and at high confining pressures. In principle, therefore, it is possible to choose a priori which model to use for the brittle and ductile end-members, but the choice is not so straightforward for intermediate materials.

With regard to the second requirement, we note that the coherence to both exponential and power laws is similar to the competition between exponential and power law forms of the velocity-stress intensity relationships in subcritical crack growth [*Atkinson*, 1987; *Lawn*, 1993]. However, it has been suggested that on physical grounds the exponential form is consistent with the reaction rate theory for the subcritical growth of a single crack [*Lawn*, 1993], whereas the power law form is more appropriate for damage mechanics involving the growth and coalescence of a crack population [*Main*, 2000]. Without the former, no cracks would grow, and without the latter we would not see the large crack densities described here.

In the case of the third requirement our data suggest that the value of β in exponential creep is not only independent of confining pressure but is also roughly constant for all the samples tested. On the other hand, the constants C (exponential creep) and A (power law creep) do vary both with confining pressure and with mechanical attributes (brittle or ductile) of the samples. We note that the confining pressure dependence of C is small relative to that of A and further that other studies have also reported strong confining pressure dependence in A [see *Ranalli*, 1995]. More importantly, both parameters (A and η) for power law creep differ markedly between brittle and ductile samples and are more sensitive to external conditions, which themselves vary with depth in the lithosphere. Therefore, while exponential and power law forms can both describe the data, only the power law form satisfies all three criteria. In subsequent discussions, we concentrate on developing the power law equation further, while bearing in mind that the same analysis can be carried out for the exponential case.

Equations (1) and (2) are constructs in the sense that a finite value of strain rate can be calculated for any stress. However, we note in Figure 2b that there is a threshold stress below which creep does not occur and the rock can never fail, i.e., $\dot{\varepsilon} = 0$. Using our externally mounted LVDT, the lowest strain rate that can be resolved is about 10^{-10} s^{-1}, but creep rates lower than this can be resolved by other techniques. *Griggs* [1940] called this stress limit the fundamental strength of the rock, in that it represents the lowest stress at which a rock can fail in the long term. Similarly, a finite minimum stress intensity is required to activate the stress corrosion mechanism for single cracks [*Atkinson*, 1987]. Ignoring this property implies that creep will occur at all nonzero stresses, which contradicts geological and engineering observations. A full description of the $\dot{\varepsilon} - \sigma_d$ data must therefore include this important property. Thus for power law creep, a more physically meaningful form of equation (1) is

$$\dot{\varepsilon} = A'(\sigma_d - \sigma_f)^{\eta'}, \tag{3}$$

where σ_f is the fundamental strength for time-dependent deformation and primes represent modified versions of those defined in (1).

A recent study by *Main* [2000] arrived at (3) purely from a theoretical standpoint. His derivation was based on a combination of nonlinear constitutive equations for time-dependent crack growth [*Atkinson and Meredith*, 1987] and local feedback mechanisms from linear elastic fracture mechanics [*Lawn*, 1993]. His aim was to link the macroscopic creep measurements to possible underlying creep mechanisms, in particular, stress corrosion. *Main* [2000] showed that steady state creep at a constant stress emerges as a consequence of competing negative and positive feedback in crack growth and need not of itself require a separate mechanism.

Table 3 shows values of the new constants A', σ_f, and η' obtained by nonlinear curve fitting of the data to (3). Of particular interest is the range of values taken by the index η' when (3) is used. In all the sandstones tested, we find $1 < \eta' < 6$, which is within the range found for power law creep by ductile mechanisms above homologous temperatures ≥ 0.4 [*Twiss and Moores*, 1992]. The highest values of η' found are for the more brittle Gyda and Magnus sandstones (Figure 7a), while the lowest values are shown by ductile Gullfaks samples. Indeed, in three cases, data for ductile samples yielded $\eta' \sim 0.5$. A generalized law for compaction creep also takes power law form, with stress exponents of about unity [*Spiers et al.*,

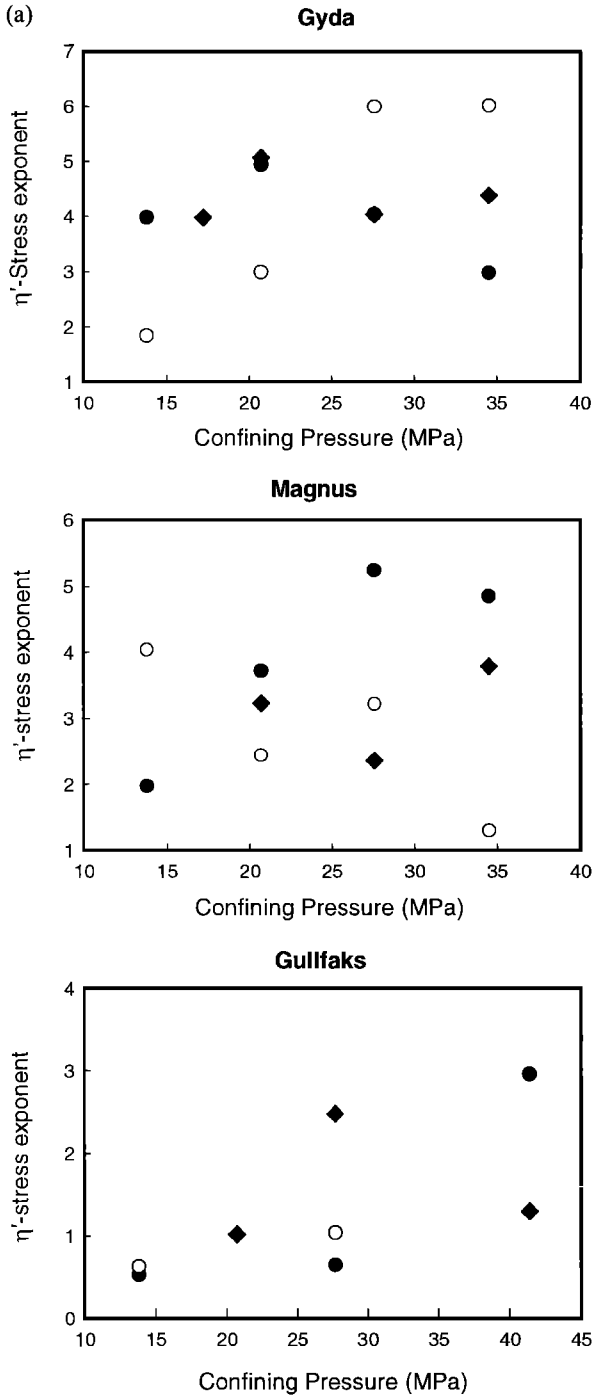

Figure 7a. Confining pressure dependence of the material constants in the modified power law relationship (equation (3)) for A'. Solid circles, 0.1 MPa; open circles, 6.9 MPa; solid diamonds, 13.8 MPa. Note that both A' and η' (Figure 7b) are much more sensitive to confining pressure.

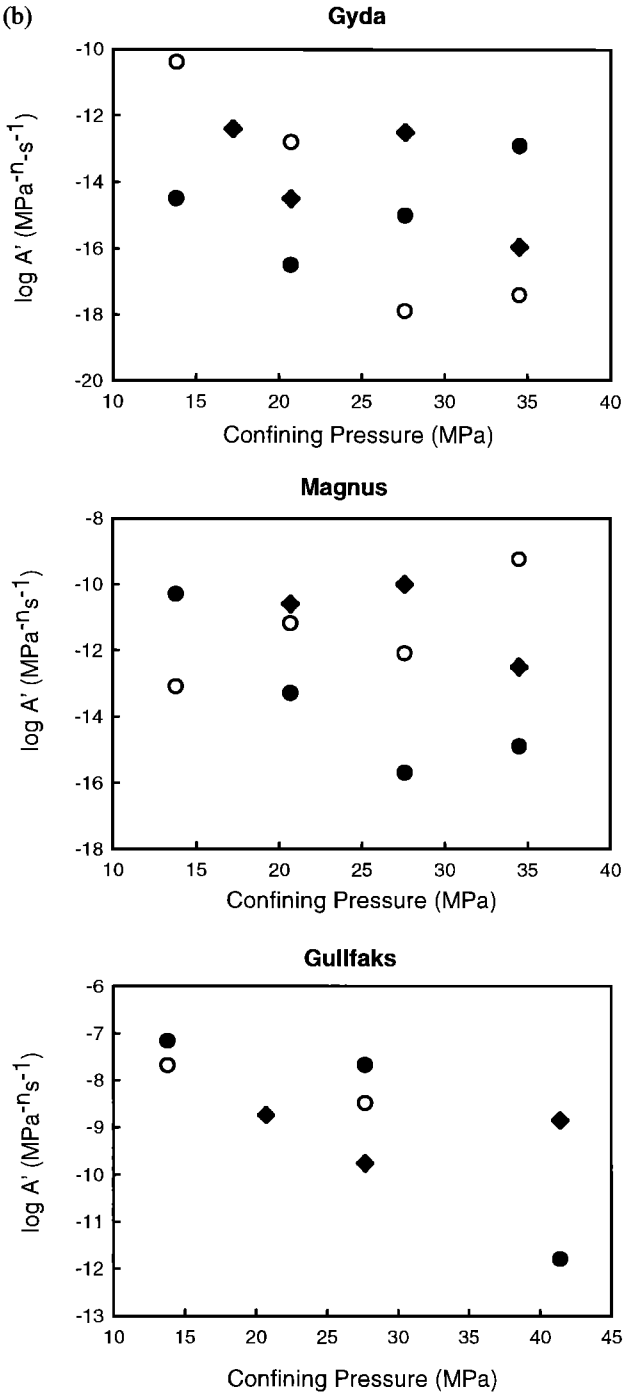

Figure 7b. Same as Figure 7a except for η'.

1990; *Paterson*, 1995]. In both cases, higher exponents in (1) or (3) are associated with relatively brittle rocks.

Comparison of (3) with the derivation of *Main* [2000] leads to the result $\eta' = n + 1$, where n is the stress corrosion index as defined for subcritical crack growth [*Charles*, 1958; *Atkinson and Meredith*, 1987]. Hence from the values in Table 3, we have $0 \leq n \leq 5$ for our suite of sandstones. The significance of this is that samples showing $n > 2$ are likely eventually to fail by localized deformation after a phase of accelerating tertiary creep [*Das and Scholz*, 1981; *Main*, 2000]. Published values of n for single cracks in brittle rocks vary from 20 to 50 for crack growth by stress corrosion [*Atkinson and Meredith*, 1987]. Nevertheless, it has also been found that when crack growth rate is limited by diffusion at the crack tip, n values decrease to between 2 and 10 [*Lockner*, 1993]. More importantly, n is also reduced to values consistent with those obtained here for the case of a population of cracks under compressive stress [*Liakopoulou-Morris et al.*, 1994]. Our data for the three reservoirs in which creep could be measured suggested higher values of η' for the more brittle Gyda samples, although this distinction

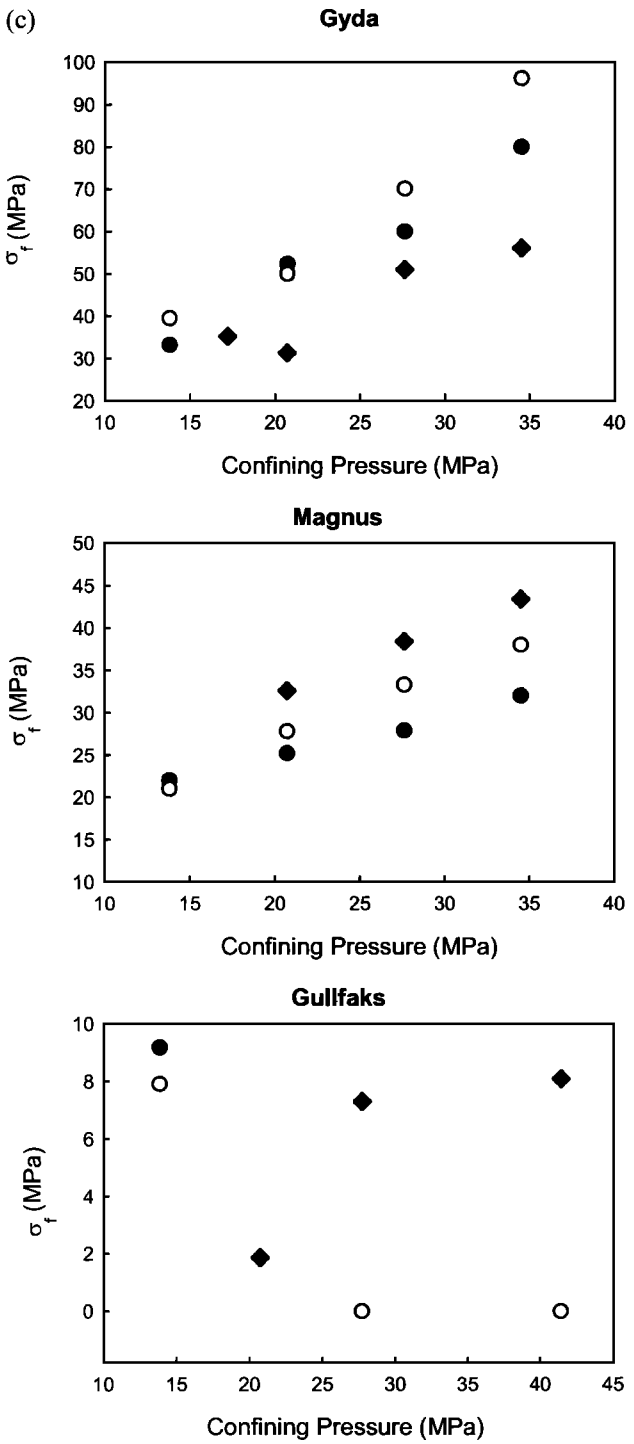

Figure 7c. Same as Figure 7a except for σ_f. The fundamental strength is also sensitive to confining pressure but only for the brittle samples, providing a means to distinguish between brittle and ductile samples.

is weak. Equally, η' values from (1) ranged from 1 to 15. Those rocks with η' in the range $3 < \eta' < 15$ are in the "unstable" regime and therefore also consistent with the findings of *Liakopoulou-Morris et al.* [1994] for the later stages of deformation.

From Figure 7b we note that the parameter A' decreases systematically with increasing confining pressure and ranges from about 10^{-7} to 10^{-18} $MPa^{-\eta'}$ s^{-1}. This confining pressure dependence is evident for equation (1) in Figure 5c, although mostly for relatively brittle samples. The fundamental strength (σ_f) increases systematically with confining pressure and is found to be a more sensitive measure of confining pressure dependence for the relatively brittle (Gyda and Magnus) samples (Figure 7c). All sandstones tested in our experiments obey (3), with modifications that can be traced to intersample variations in mechanical attributes. For ductile and weakly consolidated samples (Gullfaks), σ_f is close to zero, and the curves therefore define power law creep as in equation (1) (Figure 4c), as reported elsewhere [e.g., *Spiers et al.*, 1990]. Intuitively, we would expect this to be the case since weakly consolidated materials are unlikely to support large nonzero differential stresses. On the other hand, brittle samples have a finite σ_f and can thus support stresses below this value for an infinite time without failure (Figure 2b).

On the basis of (3) and the data for all our sandstone samples, we can define three different rheological groups based on the magnitude of σ_f relative to σ_s, where σ_s is the dry short-term failure strength. The end-members are defined by ductile sandstones which are characterized by σ_f close to zero (Gullfaks) and brittle sandstones which are characterized by $\sigma_f = \sigma_s$ (Scott). Indeed, we were unable to detect measurable creep in Scott samples except when loaded to levels very close to the short-term failure stress (Figure 8a). Between these two end-members is a range of sandstones that show mixed behavior (local compaction and dilatancy) for which $\sigma_f < \sigma_s$ (Gyda and Magnus). These groups are illustrated schematically in Figure 8b.

The question that arises from the discussion above is whether the physical model of (3) [*Main*, 2000] provides an improved statistical fit to the experimental data. Examination of Table 3 shows that the correlation coefficients for the modified equation are generally higher than those for the conventional power law creep. However, a more rigorous test is needed to judge improved model performance for the required increase in the number of adjustable parameters. This was achieved by adopting Akaike's information criterion (AIC in Table 3), which introduces a penalty for increased complexity in a mathematical model (details in work by *Main et al.* [1999]). Specifically, a three-parameter model is justified only if the $AIC_3 > AIC_2$, where the subscript is the number of parameters in the model. As shown in Table 3, this requirement does not hold since in all but two cases, $AIC_3 < AIC_2$. This is perhaps not surprising since the number of data points (five) is small compared to the number of degrees of freedom in the three-parameter equation. Three more data will therefore be needed to discriminate on statistical grounds between the competing physical models.

In summary, equation (3) provides a more physically meaningful description of the experimental data than (1), where the fundamental strength represents an important additional macroscopic constant which can be used to differentiate porous rocks on the basis of both their mechanical attributes and the underlying microscopic creep mechanisms. However, a more rigorous statistical test has shown that there are too few data points in the current study to distinguish the statistical significance of the three-parameter model at this stage.

5. Conclusions

We have presented new experimental data on the time-dependent deformation of a suite of sandstones of varying

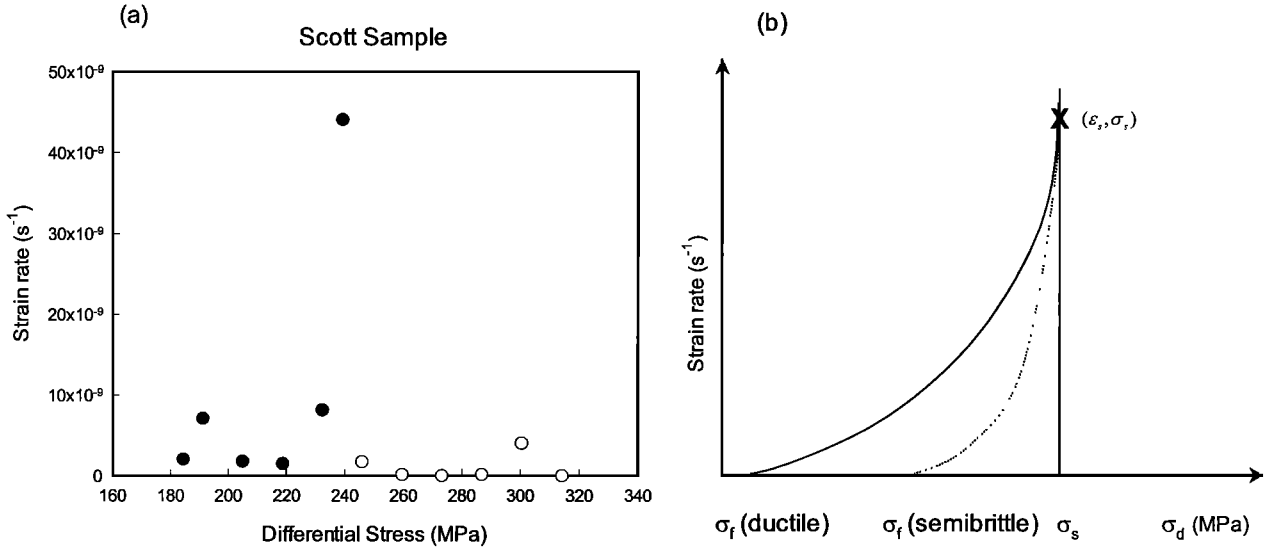

Figure 8. (a) Typical strain rate data for Scott samples, showing that creep in these extremely brittle samples was not resolvable with our technique, except when the sample was close to failure (27.6 MPa data). Confining pressures are 27.6 MPa (solid circles) and 41.4 MPa (open circles). (b) Schematic illustration of the relationship between strain rate and the fundamental strength for sandstones of contrasting rheological behavior. For convenience, the fundamental strengths are depicted relative to the short-term failure strength by assuming that the short-term strength also fits power law according to (3), albeit with different fitting parameters [*Main*, 2000].

microstructural and mechanical properties. In particular, we find that the steady state strain rate has an exponential dependence on differential stress for brittle (low porosity) samples and power law dependence for ductile (high porosity) samples. On the basis mainly of damage mechanics [*Main*, 2000] and also on the ability to distinguish between brittle and ductile sandstones, a modified form of the power law equation has been developed, which includes a parameter for the long-term fundamental strength of sandstones. This fundamental strength for time-dependent deformation varies much more than the other parameters of the distribution. However, while the new equation is physically more meaningful, more data are required to test whether the extra parameter is justified in a statistical sense.

Acknowledgments. This study was funded through the Department of Trade and Industry's Hydrocarbons LINK Programme. We are grateful to BP Amoco, Texaco, and Statoil for matching funds and for providing access to well data and reservoir samples. We would also like to thank O. Peterssen, K. Heffer, J. Curran, and N. Koustabeloulis for stimulating discussions. Our work also benefited from discussions with Karen Mair, who assisted on some of the experiments. We thank Teng-Fong Wong, Greg Hirth, and an anonymous reviewer for constructive comments that improved the clarity of our arguments. Finally, we thank Yvonne Fletcher and Louise Kerr for the photographic work and Sally Hamilton for measurements of porosity and permeability on the core plugs prior to testing.

References

Atkinson, B. K., Introduction to fracture mechanics and its geophysical applications, in *Fracture Mechanics of Rocks*, edited by B. K. Atkinson, pp. 1–26, Academic, San Diego, Calif., 1987.

Atkinson, B. K., and P. G. Meredith, The theory of sub-critical crack growth with applications to minerals and rocks, in *Fracture Mechanics of Rocks*, edited by B. K. Atkinson, pp. 111–166, Academic, San Diego, Calif., 1987.

Brace, W. F., and D. L. Kohlstedt, Limits of lithospheric stress imposed by laboratory experiments, *J. Geophys. Res.*, *85*, 6348–6252, 1980.

Brace, W. F., B. W. Paulding, and C. H. Scholz, Dilatancy in the fracture of crystalline rocks, *J. Geophys. Res.*, *71*, 3939–3953, 1966.

Charles, R. J., Fatigue of glass, I, *J. Appl. Phys.*, *29*, 1549–1560, 1958.

Costin, L. S., Time-dependent deformation and failure, in *Fracture Mechanics of Rock*, edited by B. K. Atkinson, pp. 167–215, Academic, San Diego, Calif., 1987.

Das, S., and C. H. Scholz, Theory of time-dependent rupture in the Earth, *J. Geophys. Res.*, *86*, 6039–6051, 1981.

De Meer, A., and C. J. Spiers, Creep of wet gypsum aggregates under hydrostatic loading conditions, *Tectonophysics*, *245*, 171–183, 1995.

De Meer, A., and C. J. Spiers, Uniaxial compaction of wet gypsum aggregates, *J. Geophys. Res.*, *102*, 875–891, 1997.

Dewers, T., and A. Hajash, Rate laws for water-assisted compaction and stress-induced water-rock interaction in sandstones, *J. Geophys. Res.*, *100*, 13,093–13,112, 1995.

Dunn, D. E., L. J. Lafountain, and R. E. Jackson, Porosity dependence and mechanism of brittle fracture in sandstones, *J. Geophys. Res.*, *78*, 2403–2416, 1973.

Engelder, J. T., Cataclasis and the generation of fault gouge, *Geol. Soc. Am. Bull.*, *85*, 1515–1522, 1974.

Freidman, M., and J. M. Logan, Microscopic feather fractures, *Geol. Soc. Am. Bull.*, *81*, 3417–3420, 1970.

Glover, P. W. J., J. B. Gomez, P. G. Meredith, S. A. Boon, P. R. Sammonds, and S. A. F. Murrell, Modelling the stress-strain behaviour of saturated rocks undergoing triaxial deformation using complex electrical conductivity measurements, *Surv. Geophys.*, *17*, 307–330, 1996.

Goetze, C., and B. Evans, Stress and temperature in the bending lithosphere as constrained by experimental rock mechanics, *Geophys. J. R. Astron. Soc.*, *59*, 463–478, 1979.

Gratier, J. P., and R. Guiguet, Experimental pressure solution-deposition on quartz grains: The crucial effect of the nature of the fluid, *J. Struct. Geol.*, *8*, 845–856, 1986.

Griggs, D. T., Experimental flow of rocks under conditions favouring re-crystallisation, *Geol. Soc. Am. Bull.*, *51*, 1001–1022, 1940.

Groshong, R. H., Low-temperature deformation mechanisms and their interpretation, *Geol. Soc. Am. Bull.*, *100*, 1329–1360, 1988.

Harrison, P. J., R. E. Waters, and F. J. R. Taylor, A broad spectrum of artificial seawater medium for coastal and open ocean phytoplankton, *J. Phycol.*, *16*, 28–35, 1980.

Hirth, G., and J. Tullis, The effects of pressure and porosity on the micro-mechanics of the brittle-ductile transition in quartzite, *J. Geophys. Res.*, *94*, 17,825–17,838, 1989.

Jin, Z. M., Q. Bai, and D. L. Kohlstedt, High temperature creep of olivine crystals from four localities, *Phys. Earth Planet. Inter.*, *82*, 55–64, 1994.

Kirby, S. H., and A. K. Kronenberg, Rheology of the lithosphere: Selected topics, *Rev. Geophys.*, *25*, 1219–1244, 1987.

Kohlstedt, D. L., B. Evans, and S. J. Mackwell, Strength of the lithosphere: Constraints imposed by laboratory experiments, *J. Geophys. Res.*, *100*, 17,587–17,602, 1995.

Kranz, R. L., The effects of confining pressure and stress difference on static fatigue of granite, *J. Geophys. Res.*, *85*, 1854–1866, 1980.

Lawn, B., *Fracture of Brittle Solids*, 387 pp., Cambridge Univ. Press, New York, 1993.

Liakopoulou-Morris, F., I. G. Main, B. R. Crawford, and B. G. D. Smart, Microseismic properties of a homogeneous sandstone during fault development and frictional sliding, *Geophys. J. Int.*, *119*, 219–230, 1994.

Lockner, D. A., Room temperature creep in saturated granite, *J. Geophys. Res.*, *98*, 475–487, 1993.

Lockner, D. A., A generalized law for brittle deformation of Westerly granite, *J. Geophys. Res.*, *103*, 5107–5123, 1998.

Lockner, D. A., and J. D. Byerlee, Development of fracture planes during creep in granite, in *Second Conference on Acoustic Emission/Microseismic Activity in Geological Structures and Materials*, pp. 11–25, Trans-Tech. Publ., Clausthal-Zellerfeld, Germany, 1980.

Lockner, D. A., J. D. Byerlee, V. Kuksenko, A. Ponomarev, and A. Sidorin, Observations of quasi-static fault growth from acoustic emissions, in *Fault Mechanics and Transport Properties of Rocks*, edited by B. Evans and T.-F. Wong, pp. 3–31, Academic, San Diego, Calif., 1992.

Main, I. G., Evolution of strain and seismic event rate in the transition from stable to unstable damage: Derivation of power-law 'steady-state' creep and constitutive rules for aftershock and foreshock sequences, *Geophys. J. Int.*, *142*, 151–161, 2000.

Main, I. G., T. Leonard, O. Papasouliotis, C. G. Hatton, and P. G. Meredith, One slope or two? Detecting statistically significant breaks in slope in geophysical data, with application to fracture scaling relationships, *Geophys. Res. Lett.*, *26*, 2801–2804, 1999.

Mair, K., I. G. Main, and S. C. Elphick, Sequential growth of deformation bands in the laboratory, *J. Struct. Geol.*, *22*, 25–42, 2000.

Maranini, E., and M. Brignoli, Creep behaviour of a week rock: Experimental characterisation, *Int. J. Rock Mech. Min. Sci.*, *36*, 127–138, 1998.

Marquardt, D. W., An algorithm for least squares estimation of parameters, *J. Soc. Ind. Appl. Math.*, *11*, 431–441, 1963.

Menendez, B., W. Zhu, and T.-F. Wong, Micromechanics of brittle faulting and cataclastic flow in Berea sandstone, *J. Struct. Geol.*, *18*, 1–16, 1996.

Moore, D. E., and D. A. Lockner, The role of micro-cracking in shear-fracture propagation in granite, *J. Struct. Geol.*, *17*, 95–114, 1995.

Newman, R., and N. White, Rheology of the continental lithosphere inferred from sedimentary basins, *Nature*, *385*, 621–624, 1997.

Ngwenya, B. T., S. C. Elphick, I. G. Main, and G. B. Shimmield, Experimental constraints on the diagenetic self-sealing capacity of natural faults in reservoir sandstones, *Earth Planet. Sci. Lett.*, *183*, 187–199, 2000.

Paterson, M. S., A theory for granular flow accommodated by material transfer via an inter-granular fluid, *Tectnonphysics*, *245*, 135–151, 1995.

Ranalli, G., *Rheology of the Earth*, 413 pp., Chapman and Hall, New York, 1995.

Rao, M. V. M. S., and K. Kusunose, Failure zone development in andesite as observed from acoustic emission locations and velocity changes, *Phys. Earth Planet. Inter.*, *88*, 131–143, 1995.

Roberston, E. C., Creep in Solenhofen limestone, *Mem. Geol. Soc. Am.*, *79*, 227 pp., 1960.

Rutter, E. H., Pressure solution in nature, theory and experiment, *J. Geol. Soc. London*, *140*, 725–740, 1983.

Rutter, E. H., On the nomenclature of mode of failure transitions in rocks, *Tectonophysics*, *122*, 363–387, 1986.

Rutter, E. H., and D. H. Mainprice, The effect of water on the stress relaxation of faulted and unfaulted sandstone, *Pure Appl. Geophys.*, *116*, 634–654, 1978.

Sano, O., I. Ichiro, and M. Terada, Influence of strain rate on dilatancy and strength of Oshima Granite under uniaxial compression, *J. Geophys. Res.*, *86*, 9299–9311, 1981.

Scholz, C. H., Mechanism of creep in brittle rock, *J. Geophys. Res.*, *73*, 3295–3302, 1968.

Sibson, R. H., Fault rocks and fault mechanisms, *J. Geol. Soc. London*, *133*, 191–213, 1977.

Spiers, C. J., P. M. T. M. Schutjens, R. H. Brzesowsky, C. J. Peach, J. L. Liezenberg, and H. J. Zwart, Experimental determination of constitutive parameters governing creep of rocksalt by pressure solution, in *Deformation Mechanisms, Rheology and Tectonics*, edited by R. J. Knipe and E. H. Rutter, *Geol. Soc. Spec. Publ.*, *54*, 215–227, 1990.

Twiss, R. J., and E. M. Moores, *Structural Geology*, 532 pp., W. H. Freeman, New York, 1992.

Wong, T.-F., C. David, and W. Zhu, The transition from brittle faulting to cataclastic flow in porous sandstones: Mechanical deformation, *J. Geophys. Res.*, *102*, 3009–3025, 1997.

B. R. Crawford, ExxonMobil Upstream Research Company, P.O. Box 2189, Houston, TX 77252-2189, USA. (brian.r.crawford@exxon.sprint.com)

S. C. Elphick, I. G. Main, and B. T. Ngwenya, Department of Geology and Geophysics, University of Edinburgh, West Mains Road, Edinburgh EH9 3JW, Scotland, UK. (selphick@glg.ac.uk;ian.main@glg.ed.ac.uk; bryne.ngwenya@ed.ac.uk)

B. G. D. Smart, Department of Petroleum Engineering, Heriot-Watt University, Riccarton, Edinburgh EH14 4AS, Scotland, UK. (brian_smart@pet.hw.ac.uk)

(Received April 28, 2000; revised January 29, 2001;
accepted March 28, 2001.)